ISSN 0005–1144
ATKAAF 42(3–4), 117–132 (2001)

István Nagy

Nonlinear Phenomena in Power Electronics

UDK 621.38.022:510.8
IFAC IA 4.0.1;2.1

Review

A new class of phenomena has recently been discovered in nonlinear dynamics. New concepts and terms have entered the vocabulary to replace time functions and frequency spectra in describing their behavior, e.g. chaos, bifurcation, fractal, Lyapunov exponent, period doubling, Poincaré map, strange attractor etc. The main objective of the paper is to summarize the state of the art in the advanced theory of nonlinear dynamical systems and illustrate its application in power electronics by three examples.

Key words: nonlinear dynamics, theory of chaos, routes to chaos, fractal geometry, power electronics

1 INTRODUCTION

A new class of phenomena has recently been discovered three centuries after the publication of Newton's »Principia« (1687) in nonlinear dynamics. New concepts and terms have entered the vocabulary to replace time functions and frequency spectra in describing their behavior, e.g. chaos, bifurcation, fractal, Lyapunov exponent, period doubling, Poincaré map, strange attractor etc. [1].

Until recently chaos and order have been viewed as mutually exclusive. Maxwell's equations govern the electromagnetic phenomena, Newton's laws describe the processes in classical mechanics etc. They represent the world of order, which is predictable. Processes were called chaotic when they failed to obey laws and they were unpredictable. Although chaos and order have been believed to be quite distinct faces of our world there were tricky questions to be answered. For example, knowing all the laws governing our global weather we are unable to predict it or a fluid system can turn easily from order to chaos, from laminar flow into turbulent flow.

It came as an unexpected discovery that deterministic systems obeying simple laws belonging undoubtedly to the world of order and believed to be completely predictable can turn chaotic. In mathematics, the study of the quadratic iterator (logistic equation or population growth model) $x_{n+1} = ax_n(1-n)$, $n = 0, 1, 2...$ revealed the close link between chaos and order [2]. Another very early example came from the atmospheric science in 1963; Lorenz's three differential equations derived from the Navier-Stokes equations of fluid mechanics describing the thermally induced fluid convection in the atmosphere, Peitgen et al [3]. They can be viewed as the two principal paradigms of the theory of chaos. One of the first chaotic processes discovered in electronics can be shown in diode resonator consisting of a series connection of a p-n junction diode and a 10–100 mH inductor driven by a sine wave generator of (50–100) kHz. To the best of the author's knowledge power electronics chaos has only been reported in dc-dc converters, Wood [4], Deane and Hamil [5], Ninomiya et al [6] and in the system reviewed in the papers [1, 7, 8] but it is certain that other cases will appear soon.

The chaos theory, although admittedly still young, has spread like wild fire into all branches of science. In physics it has overturned the classic view held since Newton and Laplace, that our universe is predictable governed by simple laws. This illusion has been fuelled by the breathtaking advances in computers promising ever increasing computing power in information processing. Instead just the opposite has happened. Researchers on the frontier of natural science have recently proclaimed that this hope is unjustified because a large number of phenomena in nature governed by known simple laws are or can be chaotic. One of their principle properties is their sensitive dependence on initial conditions. Although the most precise measurement indicates that two paths have been launched from the same initial condition, there are always some tiny, impossible-to-measure discrepancies that shift the paths along very different trajectories. The uncertainty in the initial measurements will be amplified and become overwhelming after a short time.

Therefore our ability to predict accurately future developments is unreasonable. The irony of fate is that without the aid of computers the modern theory of chaos and its geometry, the fractals, could have never been developed.

Modifying the parameters of a nonlinear system, the location and the number of equilibrium points can change. The study of these problems is the subject of bifurcation theory.

The existence of well-defined routes leading from order to chaos was the second great discovery and again a big surprise as the first one showing that a deterministic system can be chaotic.

The main objective of the paper is to summarize the state of the art in the advanced theory of nonlinear dynamical systems and illustrating its application in power electronics by three examples. Within the basic overview the four basic states of nonlinear systems are treated: fixed point, limit cycle, quasiperiodic state and chaotic state. There will be some words about the connection between the chaotic state and fractal geometry. The application examples from the field of power electronics are as follows: high frequency time-sharing inverter, hysteresis current control of voltage source DC-AC inverter and voltage control of resonant DC-DC converter.

2 BASICS, HISTORY [9]

The nonlinear dynamical systems are described by *nonlinear differential equations* and represented in *state (phase) space*. The *degree of freedom* of the system is the number of independent variables needed to determine the dynamical state of the system. Having two or three independent variables the state space is a plane or a three dimensional space. When the number of independent variables is $n > 3$, the state space dimension is n.

The system state in steady-state can be described by *fixed points* (also called equilibrium or stationary points) and by *limit cycles* in state-space. Beside them the system can be in *quasiperiodic* and in *chaotic* state. The system state is characterized from the initial state to any of the four states mentioned by trajectory in state-space as time evolves and in the four states as well.

The system can be *nonautonomous* and *autonomous*. The *nonautonomous* systems are described by

$$\dot{\underline{x}} = \underline{v} = \underline{f}\left(\underline{x}^*, t\right) \tag{1}$$

first order, coupled nonlinear differential equation system, where the state vector is $\underline{x}$, its time derivative $\dot{\underline{x}} = \underline{v}$ is the speed vector and their transposes are

$$\underline{x}^* = \left[x_1, x_2 \ldots x_n\right] \tag{2}$$

$$\underline{v}^* = \underline{f}^* = \left[v_1, v_2 \ldots v_n\right]. \tag{3}$$

t is time, x_1, x_2... and v_1, v_2... are the components of vector $\underline{x}$ and $\underline{v}$, respectively. Systems subject to time dependent external excitations belong to this category.

The *autonomous* systems are given by

$$\dot{\underline{x}} = \underline{v} = \underline{f}\left(\underline{x}^*\right) \tag{4}$$

nonlinear differential equation, where the time t does not appear explicitly.

The nonautonomous systems can be transformed to autonomous ones by enlarging the number of state-space variables by one.

Our discussion is confined to real, dissipative systems. The initial transient process is ignored and the system's final states are in the center of our interest. The trajectory is being directed to some point, curve, so-called *attractor* in state-space. The region containing the initial conditions giving rise to trajectories that finally reach the same attractor is the *basin of attraction* for that attractor. The system can have more than one basin of attraction. The border between two (or more) basins of attraction is called *separatrix*.

2.1 Fixed points

All the time derivatives of the state-variables are zero in fixed points for autonomous system, that is

$$\underline{f}\left(\underline{x}^*\right) = 0 \tag{5}$$

The fixed points $\underline{x}_1$, $\underline{x}_2 \ldots \underline{x}_i$ can be determined by solving the system of nonlinear algebraic equations (5). The fixed points can be stable and unstable. Assuming a state-space of three dimensions and linearizing $\underline{f}(\underline{x}^*)$ around fixed point $\underline{x}_k$, the Jacobian matrix is

$$\underline{J}_k = \begin{bmatrix} \frac{\partial f_1}{\partial x_1} & \frac{\partial f_1}{\partial x_2} & \frac{\partial f_1}{\partial x_3} \\ \frac{\partial f_2}{\partial x_1} & \frac{\partial f_2}{\partial x_2} & \frac{\partial f_2}{\partial x_3} \\ \frac{\partial f_3}{\partial x_1} & \frac{\partial f_3}{\partial x_2} & \frac{\partial f_3}{\partial x_3} \end{bmatrix} \tag{6}$$

where x_1, x_2 and x_3 are the state variables.

Moving the system by small deviation $\Delta\underline{x}_o$ from the fixed point $\underline{x}_k$, the dynamic process of the small deviation of state variables is

$$\Delta \underline{x} = e^{\underline{J}_k t} \Delta \underline{x}_o = \left[\sum_{m=1}^{3} e^{\lambda_m t} \underline{e}_{mr} \underline{e}^*_{ml} \right] \Delta \underline{x}_o \qquad (7)$$

where λ_m is the *eigenvalue*, $\underline{e}_{mr}$ and $\underline{e}_{ml}$ are the *right* and *left eigenvectors* of matrix $\underline{J}_k$, respectively. Depending on the location of the three eigenvalues, there are eight different fixed points in the three-dimensional state-space (Figure 1).

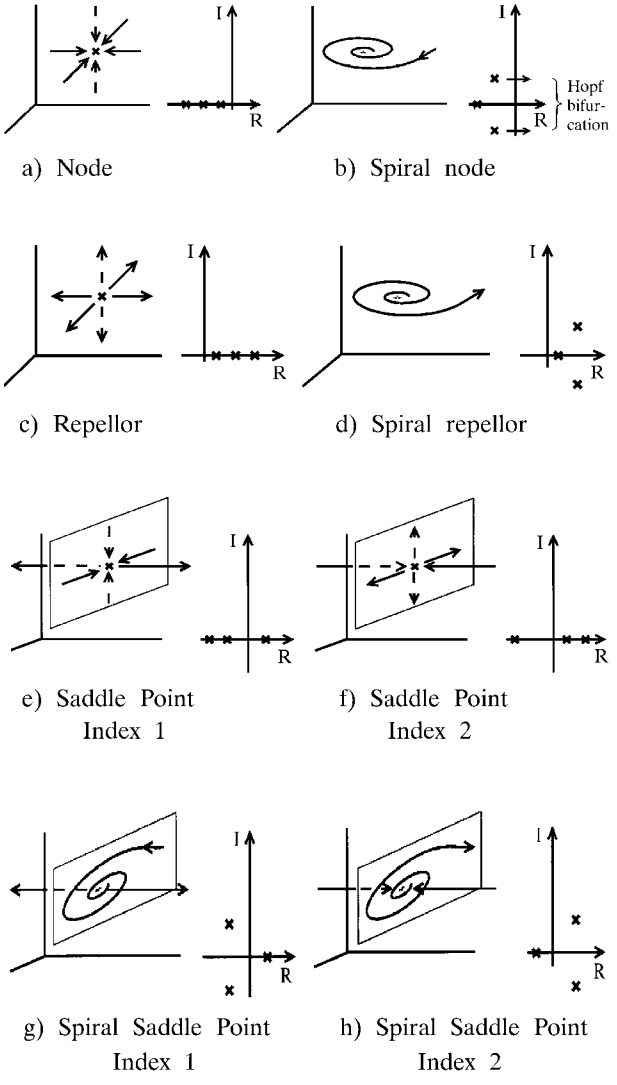

Fig.1 Classification of fixed points in 3D

The real parts of all eigenvalues are negative and the imaginary parts are zero in *node* (Figure 1a) or two of them are nonzero in *spiral node* (Figure 1b). The node and spiral nodes are stable fixed points.

The real parts of all eigenvalues are positive and the imaginary parts are zero in *repellor* (Figure 1c) or two of them (Figure 1d) are nonzero in *spiral repellor*.

Either one (Figure 1e) or two (Figure 1f) of the real parts of the three eigenvalues are positive and all imaginary parts are zero in *saddle point*.

Finally, two out of the three eigenvalues are complex conjugate pair and either one (Figure 1g) or two (Figure 1h) eigenvalues are in the right side of the complex plane in *spiral saddle point*.

The trajectories approaching to and diverging from the fixed point are shown in the figures. Trajectories heading directly toward and away from saddle point form the so-called *stable* (because $\mathrm{Re}[\lambda] < 0$ along those trajectories) and unstable *manifold*, respectively. The manifolds divide the state- -space into regions. All trajectories but the manifolds belong to one of the regions and they are confined to their own region.

2.2 Limit cycles

Periodic state, the so-called limit cycle is possible in two or higher dimensional nonlinear systems. The trajectory keeps circulating along the same closed loop in the state of limit cycle. A question of paramount importance is whether the limit cycle is stable or not. The solution can be sought by pursuing the same procedure described above. However, Poincaré discovered a simpler and more elegant approach. It uses the concept of *Poincaré section* (PS) or *map* of limit cycle and *Poincaré map function* (PMF). The Poincaré section is a set of points in the Poincaré plane (hyperplane when the dimension of state-space is higher than three, $n > 3$) produced by the trajectory by piercing through the surface from one direction (Figure 2). The selection of Poincaré plane is arbitrary.

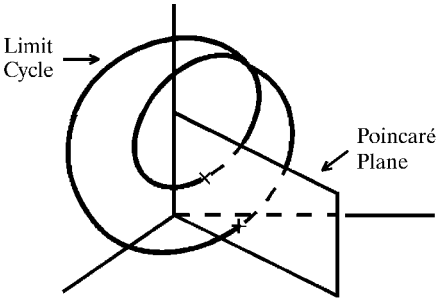

Fig. 2 Poincaré section (map) in the Poincaré plane

The five possible behaviors of the limit cycles are summarized in Figure 3.

Point P belongs to the limit cycle drawn by heavy line in all five cases. Forcing the trajectory to move by small deviation from the limit cycle, the trajectories approach to point P in an aperiodic (*node*, Figure 3a) or spiral (*spiral node* Figure 3b) way.

The limit cycle is stable. The trajectories diverge from (*repellor*, Figure 3c) or spiral around (*spiral repellor*, Figure 3d) and repelled from point P. The limit cycle in unstable. Finally, the trajectories can approach to point P in one direction and can diverge in other direction from point P (*saddle point*, Figure 3e).

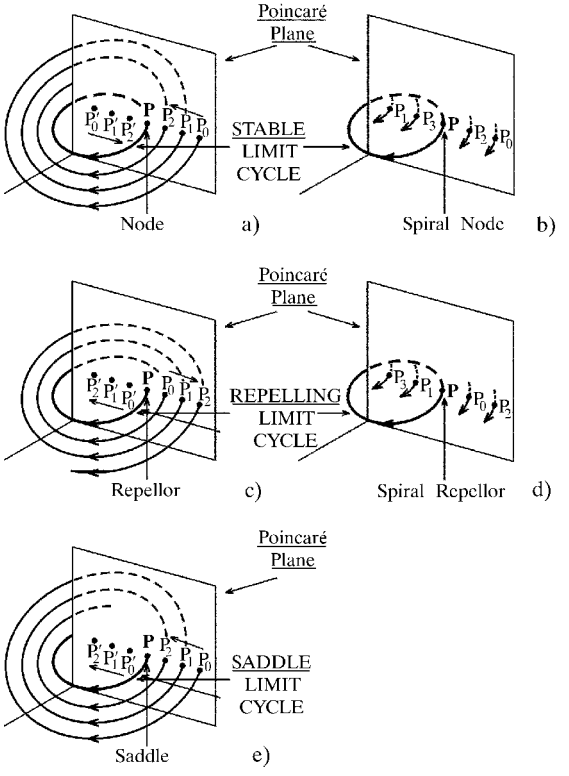

Fig. 3 Classification of fixed points

The discrete Poincaré map function (PMF) relates the coordinates of point P_n to those of the previous point P_{n-1}. All points are the crossing points in the Poincaré plane generated by the trajectory. The PMF in a three dimensional state-space is

$$x_1^{(n)} = F_1\left(x_1^{(n-1)}, x_2^{(n-1)}\right), \tag{8}$$

$$x_2^{(n)} = F_2\left(x_1^{(n-1)}, x_2^{(n-1)}\right), \tag{9}$$

where F_1 and F_2 are the PMF and x_1, x_2 are the coordinates in the Poincaré plane.

The Jacobian matrix at point P is

$$\underline{J} = \begin{bmatrix} \dfrac{\partial F_1}{\partial x_1} & \dfrac{\partial F_1}{\partial x_2} \\ \dfrac{\partial F_2}{\partial x_1} & \dfrac{\partial F_2}{\partial x_2} \end{bmatrix}. \tag{10}$$

The small deviation from point P at point P_n is

$$\Delta\underline{x}^{(n)} = \underline{J}\Delta\underline{x}^{(n-1)} = \underline{J}^n\Delta\underline{x}_o \tag{11}$$

or substituting $\underline{J}$ by its eigenvalues λ_k and right $\underline{e}_{kr}$ and left $\underline{e}_{kl}$ eigenvectors

$$\Delta\underline{x}^{(n)} = \left[\sum \lambda_n^k \underline{e}_{kr}\underline{e}_{kl}^*\right]\Delta\underline{x}_o\,. \tag{12}$$

Due to relation (12) the limit cycle is stable if and only if all eigenvalues are within the circle with unit radius.

The six possible combinations of the eigenvalues are presented in Figure 4. By changing one or more system parameters the eigenvalues can be shifted from the interior of unit circle to its border. *Bifurcation* occurs if one (or two) eigenvalue leaves the unit circle. New state(s) develops.

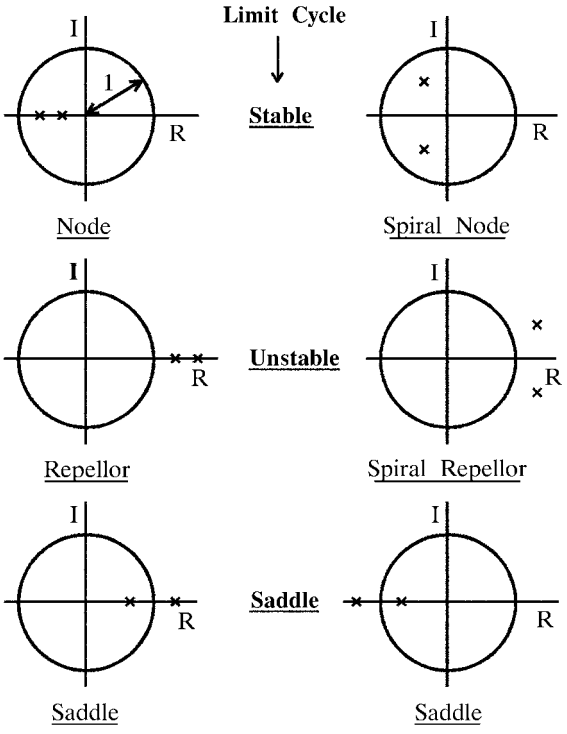

Fig. 4 Six possible locations of eigenvalues

The benefit by applying the PMF is the reduction of the dimension by one and the substitution of differential equations by difference equations.

2.3 Quasiperiodic state

The quasiperiodic state can develop if the number of state variables is three or higher. The trajectory is confined to the surface of a torus in three-dimensional state-space. The equations describing the motion of the trajectory are as follows:

$$x_1 = (R + r\sin\omega_r t)\cos\omega_R t, \quad (13)$$

$$x_2 = r\cos\omega_r t, \quad (14)$$

$$x_3 = (R + r\sin\omega_r t)\sin\omega_R t, \quad (15)$$

where x_1, x_2 and x_3 are the coordinates of the state-space, t is the time, the larger radius R is the distance of the center of the torus from the origin and the cross-sectional radius is r (Figure 5). The two angular frequencies are $\omega_R = 2\pi/T_R$ and $\omega_r = 2\pi/T_r$, where the period of rotation about the origin is T_R and that about the cross section is T_r.

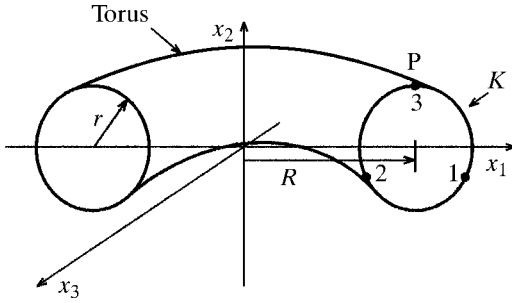

Fig. 5 The trajectory is on the surface of a torus in quasiperiodic state in three dimension

At $t = 0$ the coordinates are: $x_1 = R$; $x_2 = r$; $x_3 = 0$ and the trajectory is on the surface of the torus in point P. The trajectory will be in plane $x_1 - x_2$ after each period T_R, that is, in time $t = NT_R$, where $N = 1, 2, \ldots$

If the ratio of the two frequencies can be expressed as a ratio of two integers e.g. $\omega_r/\omega_R = 2/3$ the trajectory will repeatedly visit point P, the process is periodic. Choose the coordinate plane $x_3 = 0$ to Poincaré plane. After one, two and three period T_R the trajectory starting from point 0 at $t = 0$ makes 2/3, 4/3 and 6/3=2 turns around the small cross sections and hits point 1, 2 and 3 in the Poincaré plane (Figure 5). The Poincaré map has three discrete points on the circle of radius r phase shifted by 120 from each other. This type of process is called *frequency-locked* or *phase-locked* motion.

If the ratio of the two frequencies is irrational the trajectory on the surface of the torus will never close on itself, the process is called quasi-periodic. As $t \to \infty$ the Poincaré map will have infinite number of discrete points along the circle of radius r.

3 CHAOTIC STATE [2, 3, 9, 17, 18, 19]

The recently discovered new state is the chaotic state, which can evolve only in nonlinear systems with at least three or higher dimensions. In addition to that some other universal qualitative features common to nonlinear chaotic systems are as follows:

1. The systems are deterministic, the equations describing them are completely known.
2. They have extreme sensitive dependence on initial conditions.
3. Exponential divergence of nearby trajectories is one of the signatures of chaos.
4. Eventhough the systems are deterministic their behavior is unpredictable on the long run.
5. The trajectories in chaotic state
   – are non-periodic,
   – are bounded,
   – cannot be reproduced,
   – do not intersect each other.
6. Randomlike motion of the trajectories with underlying order and structure.

As it was mentioned the trajectories setting off from the initial conditions approach after the transient process either fixed points or limit cycles or quasiperiodic curves in dissipative systems. All of them are called *attractors* or *classical attractors* since the system is attracted to one of the above three states. When a chaotic state evolves in a system its trajectory approaches and sooner or later reaches an attractor too, the so-called *strange attractor*.

In three dimensions the classical attractors are associated with some geometric form, the stationary state with point, the limit cycle with a closed curve and the quasiperiodic state with a surface. The strange attractor is associated with a new kind of geometric object. It is called a *fractal structure*.

3.1 Routes to chaos

One of the great achievements of the theory of chaos is the discovery of several typical routes from regular states to chaos. The amazing fact is the universality of the routes to chaos. Quite different systems in their physical appearance exhibit the same route.

There are two broad classes of transitions to chaos: the *local* and *global bifurcations to chaos*. In the first case one limit cycle loses its stability. The local bifurcation has three subclasses: *period doubling*, *quasi-periodicity* and *intermittency*. The most frequent route is the period doubling. In the global bifurcation more fixed points and/or limit cycles lose its stability. It has two subdivisions the *chaotic transient* and the *crisis*.

Here only the local bifurcations and mainly the period doubling route is treated. Only one short comment is made on the quasi-periodic route and the intermittency. As a result of alteration in a parameter the system state changes first from fixed point to limit cycle through bifurcation. Later in addition another frequency develops by a new bifurcation and the system exhibits quasiperiodic

state. In other words, there are two complex conjugate eigenvalues within the unit circle. By changing further the parameter eventually the chaotic state is reached from the quasiperiodic one.

In the intermittency route to chaos apparently periodic and chaotic states are alternately developed. The system state seems to be periodic in certain intervals and suddenly it turns into a burst of chaotic state. The irregular motion calms down and everything starts again. Changing the system parameter further the length of chaotic states become longer and finally the »periodic« states are not restored.

Considering now the period-doubling route, let us assume a limit cycle as starting state in a three dimensional system (Figure 6a). The trajectory crosses the Poincaré plane at point P. As a result of changing one system variable the eigenvalue of the Jacobian matrix of PMF leaves the unit circle (Figure 6b) and a new limit cycle develops. The Poincaré plane is crossed by the new trajectory twice in one period.

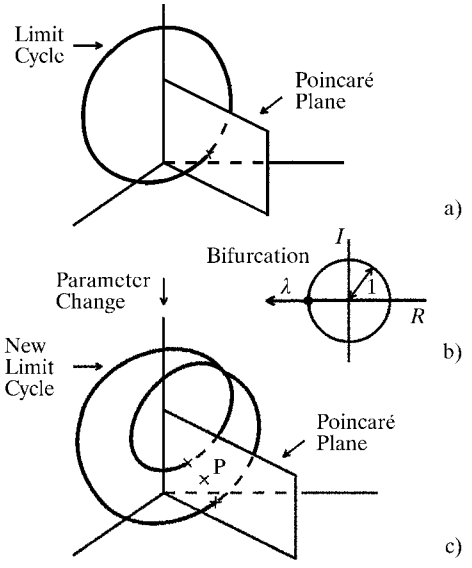

Fig. 6 Period doubling

Continuing the parameter change, new bifurcation occurs and the trajectory will cross the Poincaré plane four times (2*2) in one period instead of twice. The period doubling process keeps going on without limit.

3.2 Period doubling scenario

The period doubling scenario is shown in Figure 7 where x is the system parameter, y is one coordinate of the intersection point of the trajectory in the reference frame of the Poincaré plane. In other words y is one of the system state variables. The system state after the transient process is shown in the figure.

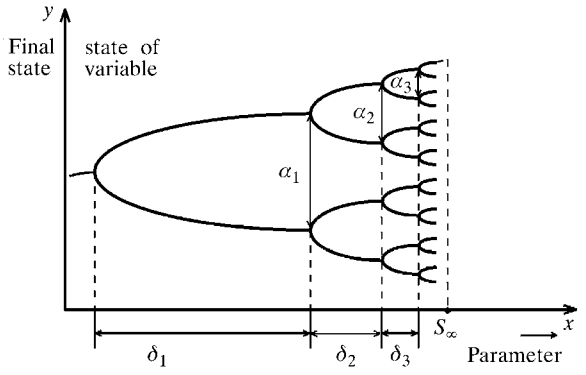

Fig. 7 Scenario of period doubling

They are called *bifurcation* or *final state diagram*. Feigenbaum has shown that the ratio of the distances δ_n between successive bifurcation points measured along the parameter axis x approaches to a constant number as the order of bifurcation, labeled by n, approaches infinity;

$$\delta = \lim_{n\to\infty} \frac{\delta_n}{\delta_{n+1}} = 4.66920161 \qquad (16)$$

where δ is the so-called Feigenbaum constant.

It is found that the ratio of the distances α_n measured in the axis y at the bifurcation points approached another constant number, the so-called Feigenbaum α

$$\alpha = \lim_{n\to\infty} \frac{\alpha_n}{\alpha_{n+1}} = 2.5029 \qquad (17)$$

Both δ and α are universal constant in the theory of chaos like other fundamental numbers, for examples, $e = 2.718 \ldots$, π and the golden mean ratio $\left(\sqrt{5}-1\right)/2$.

3.3 Examples for period-doubling route and chaotic state

Two examples well known from literature are mentioned. The first example is computer result, the second one is test result.

The quadratic iterator (or logistic equation or population growth model) is

$$x_n = a x_{n-1}(1 - x_{n-1}) \qquad (18)$$

where $n = 1, 2, \ldots$ and the parameter a can change in the range $0 \le a \le 4$. Neglecting $x = 0$, there is one single final value for x_n in the range $0 < a \le 3$ (Figure 8).

The period-doubling scenario starts from $a = 3$. First there are two final values. Substituting the smaller final value into eq. (18) as x_{n-1}, the higher final value is obtained as x_n and vice versa. A second

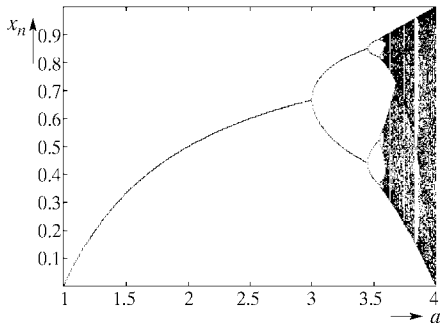

Fig. 8 Final state diagram for quadratic iterator

period-doubling occurs simultaneously both in the higher and the lower value of x_n around $a \cong 3.5$. Now there are four final values for x_n. The structure of the period-doubling scenario in Figure 8 corresponds to the one in Figure 7. The branches in the period-doubling cascade become shorter and shorter as a is increased governed by the Feigen-baum constant δ. The end of the period-doubling range is the Feigenbaum point $s_\infty = 3.5699\ldots$ From the right of point s_∞ the chaotic domain is located. It contains not simply only chaotic states but the so-called band splitting and window periodicity governed once again by the Feigenbaum constant and point. The description of them is out of the scope of the present paper. Nevertheless another property of the bifurcation diagram, the self-similarity will briefly be discussed here. Figure 9a presents once more the bifurcation diagram with a rectangular window. Magnifying the part of the diagram included in the window and turning it around the axis x by 180 , the result can be seen in Figure 9b. The similarity between Figure 9a and 9b is obvious. Following the same procedure with the part of the diagram included in the rectangular window in Figure 9b and later in Figure 9c which has been done with the part in the window of Figure 9a, Figure 9c and Figure 9d are obtained. All of the sequence of close-ups are similar to each other. The sequence of close-ups could be continued without limit and the succeeding close-ups would be always similar. Fig.9 demonstrates the self-similarity of the bifurcation diagram of the quadratic iterator. As it will be shown the fractals have self-similar structures as well.

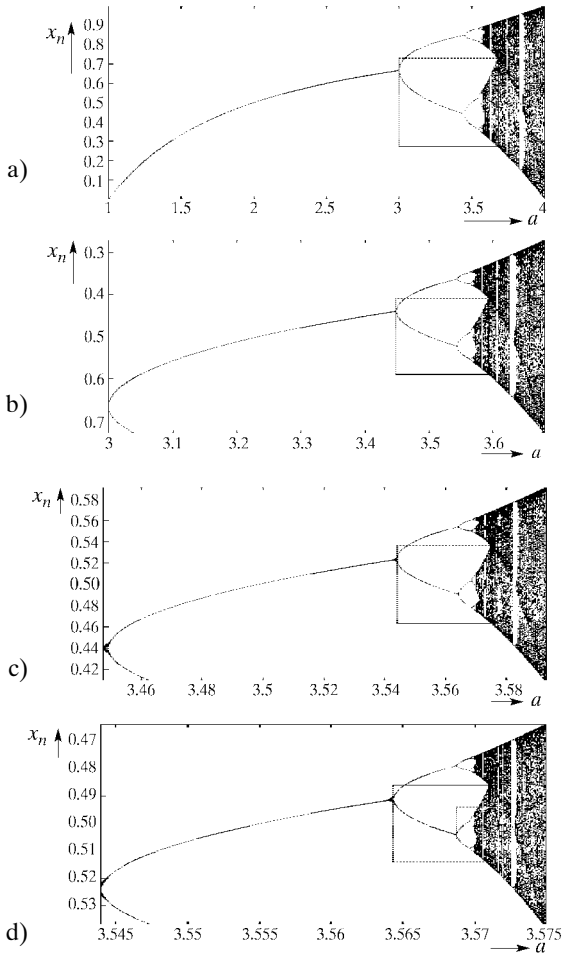

Fig. 9 Bifurcation diagrams

The second example is concerned with a simple electric circuit consisting of series *R-L* components and the nonlinear p-n junction supplied by a sinusoidal voltage source (Figure 10a). Its bifurcation diagram measured is shown in Figure 10b. The instantaneous value of the current sampled at instant of peak value of driving voltage V_{peak} is plotted on the vertical axis against V_{peak}. The period-doubling scenario and the chaotic domain are beautifully visible.

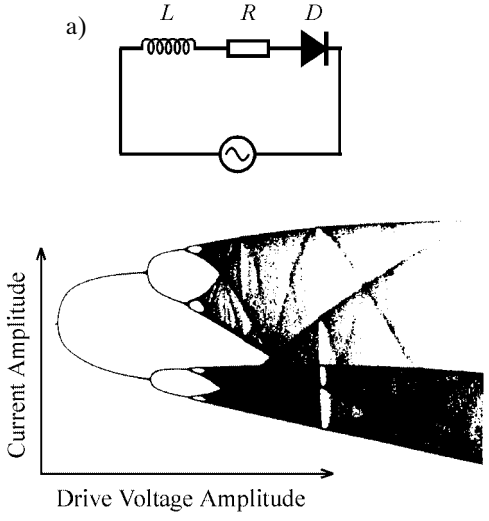

Fig. 10 Electric circuit tested (Figure 9a). Bifurcation diagram measured (Figure 9b) [20]

3.4 Quantities characterizing chaos

Similarly to the Feigenbaum constant δ and α characterizing the period-doubling route, chaos can be quantified. The first motivation for the desire to quantify chaos is to make sure whether or not the system is in chaotic state. We have to be able to make distinction between noisy and chaotic system response. The chaotic systems can be classified by quantifying them. Furthermore the changes in the behavior of the physical system can be correlated with the modification of the quantifier. Some of the most frequently applied quantifiers of chaos are: Lyapunov exponent, fractal dimension, Kolmogorov entropy and correlation dimension. The first two will be treated here in some detail.

3.4.1 *Lyapunov exponent (L.e.)*

Conceptually the L.e. is a quantitative test of the sensitive dependence on initial conditions of the system. It was stated earlier that one of the properties of chaotic systems is the exponential divergence of nearby trajectories. The calculation methods usually apply this property to determine the Lyapunov exponent λ.

After the transient process the trajectories always find their attractor belonging to the special initial condition in dissipative systems. In general the attractor as reference trajectory is used to calculate λ. Starting two trajectories from two nearby initial points placed from each other by small distance d_o, the distance d between the trajectories is given by

$$d(t) = d_o e^{\lambda t} \tag{19}$$

where λ is the Lyapunov exponent. One of the initial points is on the attractor. The equation can hold true only locally because the chaotic systems are bounded, that is, $d(t)$ cannot increase to infinity. The value λ may depend on the initial point on the attractor. To characterize the attractor by a Lyapunov exponent, the calculation described above has to be repeated for a large number of n of the initial points distributed along the attractor. Eventually the average Lyapunov exponent $\bar{\lambda}$ calculated from the individual λ_s will characterize the attractor. The criterion for chaos is $\bar{\lambda} > 0$. When $\bar{\lambda} \le 0$ the system is in regular state.

3.4.2 *Fractal dimension*

The dimensionality of geometric objects in Euclidean geometry is commonly used. The dimensionality is equal to 0 for a point, 1 for a line or closed curve, 2 for a surface and 3 for a volume. In theory dimensionality $n = 4{,}5\ldots$ is associated to hypervolumes.

It came as a surprise to almost everyone that the dimensionalities of certain geometric objects are not integers. These geometric objects are called *fractals*, because their dimensionalities are not integer.

Several definitions for the calculation of dimension exist leading to somewhat different numerical results. Only one of the measures for dimensionality the so-called *box counting dimension* D_b applied first by Kolmogorov is treated here.

The definition of D_b is as follows: use boxes of side length b to cover the space totally occupied by the object. The boxes are line segments for a curve, squares for surface and cubes for space of side length b, and so on. If the number of boxes needed to cover the geometric object is n the box counting dimension is

$$D_b = -\lim_{b\to 0} \frac{\log n}{\log b}. \tag{20}$$

As an example, apply this definition to a point. Only one square of side length b is needed to cover the point. Being $n = 1$, for the dimension $D_b = 0$ is obtained just as it was expected.

Taking a line segment of length l as geometric object, we need $n = l/b$ number of boxes to cover the line l. Applying again equation (20)

$$D_b = -\lim_{b\to 0} \frac{\log l/b}{\log b} = -\lim_{b\to 0} \frac{\log l - \log b}{\log b} = 1$$

Again the result is the expected one.

Let us consider two famous fractal objects: the *Cantor set* and the *Koch curve*. As we will see the fractal dimension D_b for the first one is in the range $0 < D_b < 1$ and for the second one $1 < D_b < 2$.

The construction of the *Cantor set* is shown in Figure 11.

The construction begins with a line segment of length 1. Infinite number of stages is needed. In the first stage of construction the middle third of the line segment is deleted. Two segments with length 1/3 each have remained. In the second stage the middle third of each line segment is removed again. Now we have $2^2 = 4$ number of segments with length $(1/3)^2$ each. In stage n the middle third of each remaining line segment is deleted. The number of segments is 2^n and their length is $(1/3)^n$. The construction of Cantor set is completed by $n \to \infty$. The number of boxes needed for the calculation of the fractal dimension D_b is 2^n and the side length of boxes is $(1/3)^n$, that is,

$$D_b = -\lim_{b\to 0} \frac{\log 2^n}{\log (1/3)^n} = -\lim_{n\to\infty} \frac{\log 2}{\log 3} = 0.63\ldots$$

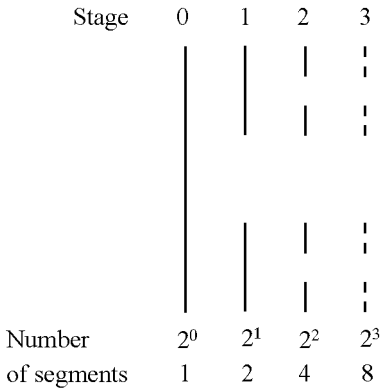

Fig. 11 Construction of the Cantor set

The fractal dimension D_b for the Cantor set is a noninteger and higher than 0 and less than 1. The Cantor set is more than a set of points but less than a line segment.

Our second example for the fractals is the Koch curve. It is a nowhere differentiable, continuous curve of infinite length. Its construction is illustrated in Figure 12.

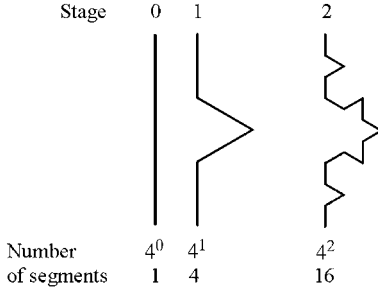

Fig. 12 Construction of Koch curve

Again we start with a straight-line segment of unit length. The middle third of the segment is replaced with two lines of length 1/3 to form a »tent«. In the second stage the middle third of each segment is replaced with two more lines to form four tents. In stage n of the construction there will be 4^n segments each of length $(1/3)^n$. The box counting dimension of the Koch curve is

$$D_b = -\lim_{b\to 0} \frac{\log 4^n}{\log(1/3)^n} = \lim_{n\to\infty} \frac{\log 4}{\log 3} = 1.26\ldots$$

As $D_b > 1$, therefore the Koch curve is more than a curve but less than a surface.

Starting from an equilateral triangle and constructing a Koch curve on each side of the triangle, the so-called *Koch snowflake* is obtained. It encircles a finite area but the length of its boundary is infinite.

Table 1 lists some Euclidean and fractal dimensions. The fractal dimension of the strange attractor of the quadratic iterator belongs to the Feigenbaum point $a = s_\infty = 3.5699\ldots$

Table 1 **Euclidean and fractal dimensions of special objects**

	Euclidean dimension		Fractal dimension
Point	0	Cantor set	0.63…
Curve	1	Koch curve	1.26…
Surface	2	Spierpinszki carpet	1.89…
Space	3	Strange attractor of quadratic iterator	0.5388…
Hyperspace	n = 4, 5…		

Why are we concerned with the fractals and fractal dimension? The answer is simple and reassuring. *The strange attractors are fractals, they have noninteger dimension*. In other words, a quantitative measure for chaos is that its attractor has noninteger dimension.

4 NONLINEAR SYSTEMS IN POWER ELECTRONICS

Three examples are shown for nonlinear dynamical systems in power electronics. The systems are piece-wise linear ones. The nonlinearity is introduced by the dependence of switching times on the hi-story of one or more state variables.

The first example is a high frequency, time-sharing inverter. It can develop various subharmonic states beside the normal fundamental periodic one. The second example is a hysteresis current controlled three-phase voltage source converter. The last example is a dual channel resonant dc-dc converter. Its output voltage is controlled by a feedback loop applying PWM switching. In the last two examples chaotic state can evolve beside the periodic and subharmonic states.

4.1 High frequency time sharing inverter [10, 11]

Figure 13 shows the inverter configuration in its simplest form.

I_+ and I_- so-called positive and negative subinverters are encircled by dotted lines. The parallel oscillatory circuit L_p-C_p-R_p represents the load. The supply is provided by a center-tapped DC voltage source.

In order to explain the mode of action of the inverter ideal components are assumed.

The basic operation of the inverter can be understood by the time functions of Figure 14. In

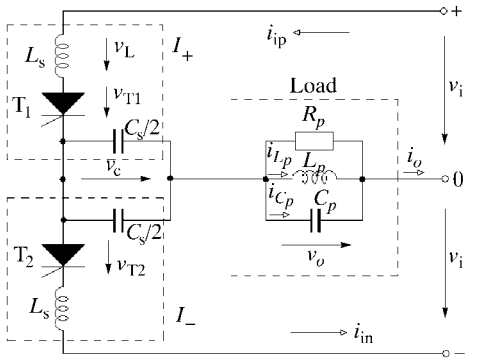

Fig. 13 The basic configuration of the inverter

Figure 14a the approximately sinusoidal output voltage v_o, the inverter output current pulses i_o, and the condenser voltage v_C can be seen.

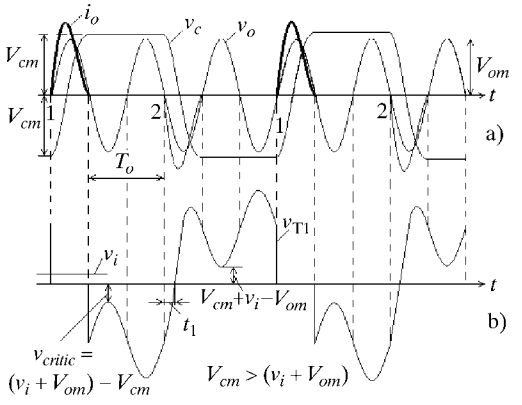

Fig. 14 Time functions in basic operation

Thyristors T1 and T2 are alternately fired at instants located at every sixth zero crossings on the positive and on the negative slope of the output voltage, respectively. After firing a thyristor, an output current pulse i_o is flowing into the load which changes the polarity of the series condenser voltage v_c, for instant from $-V_{cm}$ to V_{cm}. The thyristor turn-off time can be a little bit longer than two half cycles of the output voltage (Figure 14b).

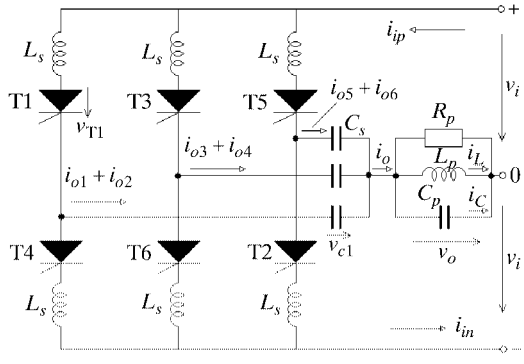

Fig. 15 The power circuit of the time-sharing inverter

Figure 15 presents the configuration having three positive and three negative subinverters. Here the respective input and output terminals of the subinverters are paralleled. The numbering of the subinverters corresponds to the firing order. Each subinverter pair works in the same way as it was previously described.

4.1.1 *Analysis*

One of the most interesting results is that *by using an approximate model assuming sinusoidal output voltage no steady-state solution can be found for the current pulse* and other variables e.g. in certain operation region [10]. The laboratory tests verified this theoretical conclusion.

To discover the phenomena in the region a more accurate model must be used. The independent energy storage elements are: six L_s series inductances, three C_s series capacitances, one L_p inductance and one C_p capacitance, altogether eleven elements, with eleven state variables. The accurate analysis was performed by simulation in Matlab environment for open and for closed loop control.

Open loop control [10]: Bifurcation diagram was generated here, the peak values of the output voltage V_{om} were sampled, stored and plotted as a function of the control parameter T_o, where T_o is the period between two consecutive firing pulses in the positive or in the negative subinverters (Figure 16).

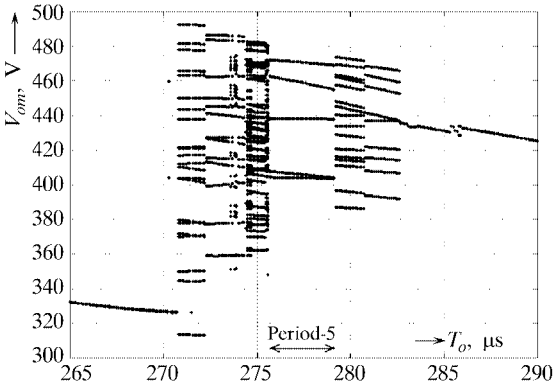

Fig. 16 Bifurcation diagram of inverter with open loop control

Having just one single value V_{om} for a given T_o, the output voltage v_o repeats itself in each period T_o. This state is called period-1. Similarly, state »period-5« develops for example at firing period $T_o = 277$ μsec. Now there are five consecutive distinct V_{om} values. v_o is still periodic, it repeats itself after $5T_o$ has been elapsed (Figure 17).

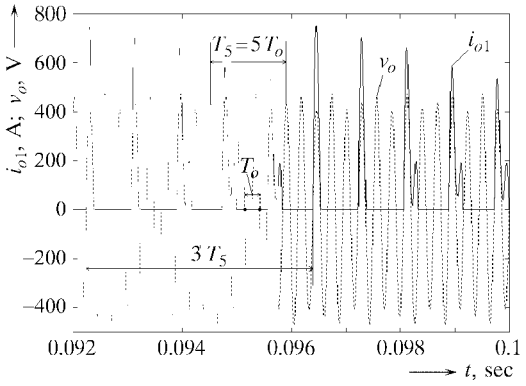

Fig. 17 $v_o(t)$ and $i_{o1}(t)$. $T_o = 277$ μs. State: Period-5.

Closed loop control [11]: A self-control structure is obtained by applying a feedback control loop. Now the approximately sinusoidal output voltage v_o is compared with a DC control voltage V_{DC} and the thyristors are alternatively fired at the crossing--points of the two curves. The study is concerned with the effect of the variation of the DC control voltage level on the behavior of the feedback-controlled inverter. Again the bifurcation diagram is used for the presentation of the results (Figure 18): the peak values of the output voltage V_{om} were sampled, stored and plotted as a function of the control parameter V_{DC}.

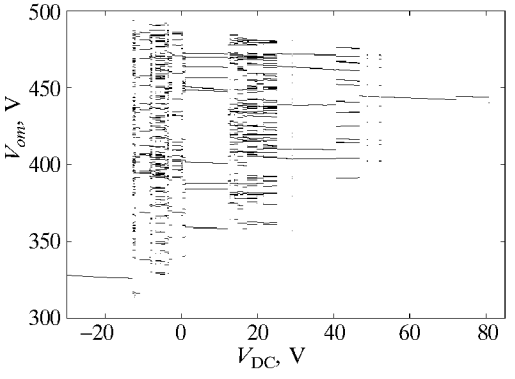

Fig. 18 Bifurcation diagram of inverter with feedback control loop

The results are basically similar to those obtained for open loop control. As in the previous study, the feedback-controlled inverter generates subharmonic as the DC voltage level is varied.

4.2 Hysteresis current controlled three phase voltage source converter [1, 7, 8]

The objective is to highlight the complex behavior of a three phase DC-AC Voltage Source Converter (VSC) controlled by a closed loop Hysteresis AC Current Controller (HCC). The block diagram of the system is shown in Figure 19. It is a somewhat sophisticated hysteresis AC current control loop. It consists of a three-phase voltage source converter, a simple circuit modeling the AC side, a reference frame transformation, a comparator and the hysteresis AC current controller.

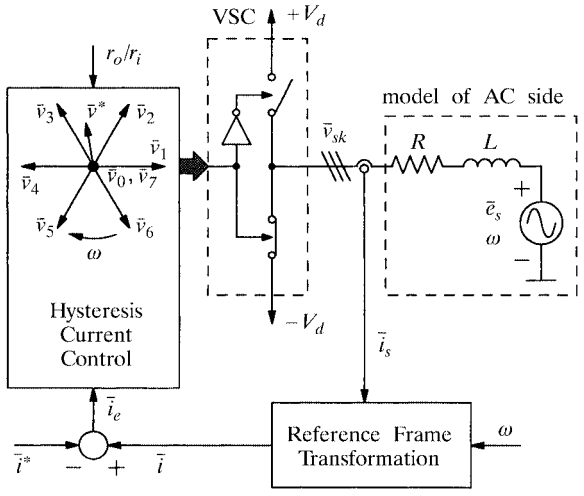

Fig. 19 Voltage source converter with its hysteresis AC current controller

All voltage and current vectors used are three phase space vectors. Space vectors with suffix s are written in Stationary Reference Frame (SRF). The three phase AC terminals of the VSC are tied through series L-R components to voltage space vector $\bar{e}_s$ rotating with angular speed ω. This simple circuit can model either the AC mains or an induction motor.

There are some benefits by using Rotating Reference Frame (RRF) over SRF. Space vectors without suffix s are in RRF.

Firstly, the AC current $\bar{i}_s$ is transformed into RRF revolving with angular frequency ω. In RRF the reference current $\bar{i}^*$ is a stationary space vector. The shape of the Tolerance Band (TB) centered around the end point of $\bar{i}^*$ is assumed to be a circle. The HCC selects the switching state of the VSC to keep the space vector of error current $\bar{i}_e = \bar{i} - \bar{i}^*$ within the TB. Whenever $\bar{i}_e$ reaches the periphery of TB a new converter voltage $\bar{v}_k$ is produced by the new switching state of VSC. The new $\bar{v}_k$ forces to rebound $\bar{i}_e$ from the periphery of TB to the interior of TB. To avoid certain shortcomings two concentric circles as TBs are applied with radius r_i and r_o ($r_o > r_i$).

Figure 20 shows a small part of the bifurcation diagram of the system. The sample points of the real component of the error current vector $\bar{i}_e$ are on

the vertical axis. T_s is the sampling time which is the sixth of the period of vector $\bar{e}_s$, $m = 1, 2\ldots$ The control parameter is r_o/r_i.

Figure 20 presents a beautiful period doubling cascade. Proceeding from right to left, after a short chaotic range suddenly the system response becomes periodic from $r_o/r_i \cong 1.1349$ to 1.1307. Starting from the latter value down to $r_o/r_i \cong 1.1281$ the period is doubled. The response remains periodic with 2nd-order subharmonic oscillation. Period doubling occurs again from $r_o/r_i \cong 1.1281$ and 4th-order subharmonic appears. After a series of period-doubling at successively closer border values of r_o/r_i the system trajectory finally becomes chaotic. Figure 20b presents the Lyapunov exponent for the region of the period doubling cascade showing again that at the bifurcation points the Lyapunov exponent becomes zero.

Systems in chaotic states are characterized by a special discrete modeling technique, the so-called Poincaré map. The Poincaré map is obtained by sampling the trajectory of the continuous system at time as it intersects a suitable chosen hyperplane.

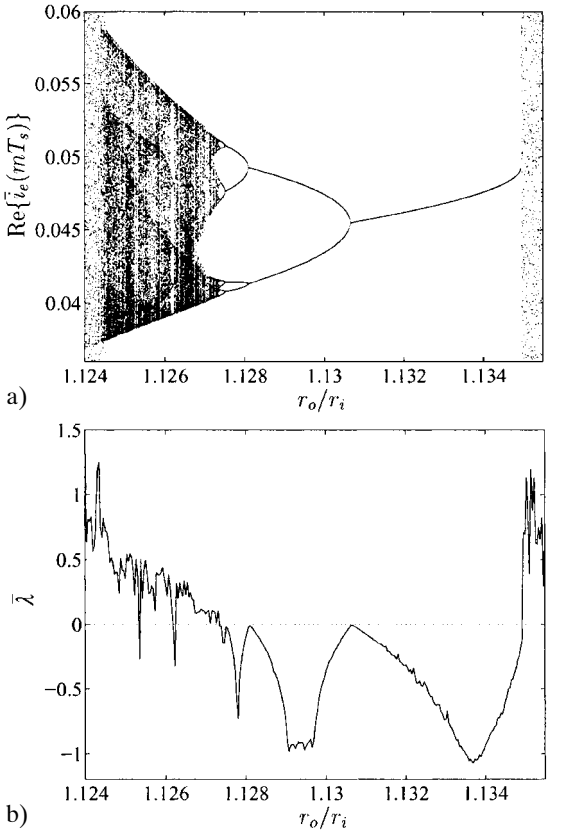

Fig. 20 (a) Period doubling cascade (b) Lyapunov exponent

With periodic forcing, like in our system the Poincaré map does not differ from the sampling of the system trajectory with a properly chosen sampling period T_s. T_s is usually selected for the period of the forcing signal. The effect of this sampling is similar to a stroboscope flashing. Periodic steady-state with period T_s is thereby represented by a single *fixed point* $\bar{x}^*$ in the Poincaré map, that is, $\bar{x}^* = P(\bar{x}^*)$. K^{th}-order subharmonic solutions with period KT_s correspond to fixed points $\{\bar{x}_1^*, \ldots, \bar{x}_K^*\}$, where $\bar{x}_1^* = P(\bar{x}_K^*)$. For chaotic state, plotting the sequence of two arbitrarily chosen components of the Poincaré map samples, a set of organized points are obtained always in the reference frame of the two components reflecting a multilayered structure and order. The Poincaré map of our system is shown in Figure 21.

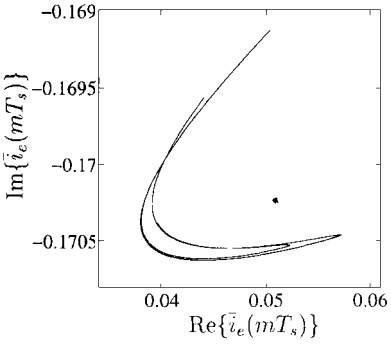

Fig. 21 Poincaré map

The structure and order of the map can be considered as an outcome of the deterministic background of chaotic systems.

4.3 Dual channel resonant DC-DC converter

[12, 13, 14, 15, 16]

The dual channel resonant DC-DC converter family was introduced earlier [12]. The family has twelve members. A common feature of the different entities is that they transmit power from input to output through two channels, the so-called positive and negative ones, coupled by a resonating capacitor. The converter can operate both in symmetrical and in asymmetrical mode. The respective variables in the two channels vary symmetrically or asymmetrically in the two modes. The energy change between the two channels is accomplished by a capacitor in asymmetrical operation. There is no energy exchange between the positive and the negative channels in the symmetrical case. Our investigation is restricted to the buck configuration (Figure 22) in symmetrical operation.

Suffix i and o refer to input and output while suffix p and n refer to positive and negative channel, respectively.

Two different converter versions can be derived from the configuration. The first version contains

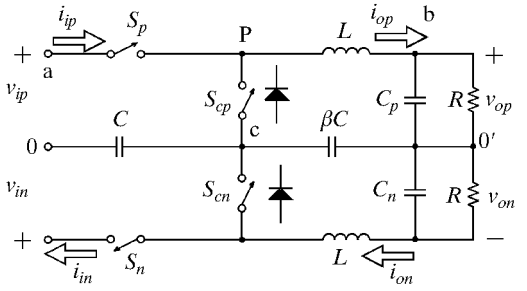

Fig. 22 Resonant buck converter with double load

diodes in place of clamping switches S_{cp} and S_{cn}. The second one applies controlled switches conducting current in the direction of arrow. The study will be confined to the case when capacitance βC is replaced by short circuit and S_{cp}, S_{cn} are applied.

The controlled switches within one channel are always in complementary states (that is, when S_p is on, S_{cp} is off and vice versa). By turning-on switch S_p, a sinusoidal current pulse i_{ip} is developed from $\omega t = 0$ to $\alpha_p \left(\omega = 1/\sqrt{LC}\right.$ in circuit S_p, L, v_{op}, C and V_{ip} (Figure 23). The currents are $i_{ip} = i_{op} = i_{cp}$ in interval $0 \le \omega t \le \alpha_p$. The capacitor voltage v_c swings from V_{cn} to V_{cp} ($V_{cn} < 0$). By turning-on switch S_{cp} at α_p the choke current commutates from S_p to S_{cp}. The energy stored in the choke at is depleted in the interval $\alpha_p < \omega t < \omega T_s$ where $T_s = 1/f_s$ is the switching period. At discontinuous current conduction (DCM) the stored energy is entirely depleted in interval $\alpha < \omega t < \alpha_{ep}$, where α_{ep} denotes the extinction angle of the inductor current. In DCM the current is zero between α_{ep} and ωT_s. In the continuous-conduction mode (CCM) of operation the inductor current flows continuously ($i_{op} > 0$). The inductor current i_{op} decreases in both cases in a linear fashion. After turning-on S_{cp} the capacitor voltage v_c stops changing. It keeps its value V_{cp}.

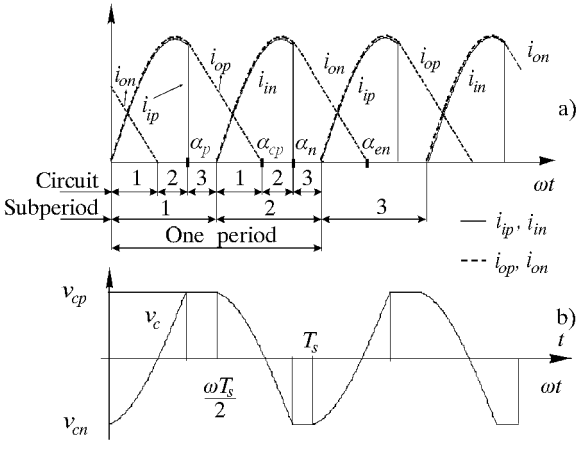

Fig. 23 Time functions of input and output currents and condenser voltage

The same process takes place at the negative side resulting in a negative condenser current pulse and voltage swing after turning-on S_n.

For controlling the output voltage $v_o = v_{op} + v_{on}$ by PWM switching, a feedback control loop is applied (Figure 24a). The control signal v_{con} is compared to the repetitive sawtooth waveform (Figure 24b). The control voltage signal v_{con} is obtained by amplifying the error, or the difference between the actual output voltage v_o and its desired value V_{ref}. The feedback loop has been left uncompensated.

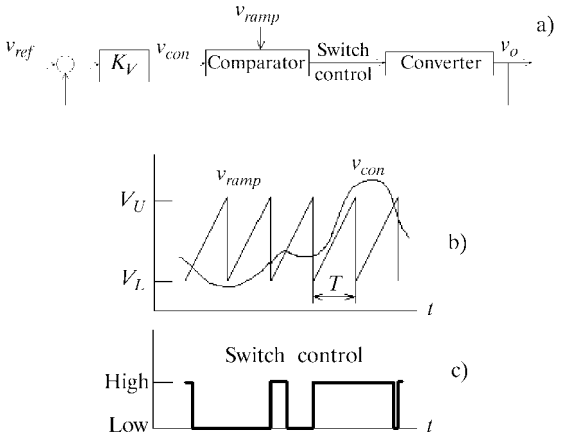

Fig. 24 PWM control: block diagram & comparator signals

When the amplified error signal v_{con} is greater than the sawtooth waveform, the switch control signal (Figure 24c) becomes high and the selected switch turns on. Otherwise, the switch is off. The controlled switches are S_p and S_n (the switches within one channel, e.g. S_p and S_{cp} are in complementary states) and they are controlled alternatively, that is the switch control signal is generated for the switch in one channel in one period of the sawtooth wave and in the next period the signal is generated for the switch in the other channel. The switching frequency of these switches is half of the frequency of the sawtooth wave.

The objective is the calculation of the variables in the feedback loop in steady-state in order to discover the various possible states of this nonlinear variable structure dynamic system. The analysis was performed by simulation in Matlab environment.

The effect of variation K_V was studied. A representative bifurcation diagram is shown in Figure 25.

To generate this kind of diagram, the output voltage v_o was sampled and stored, in steady-state, at the start of every switching cycle ($v_{ok} = v_o(kT_s)$). With sufficient number of sets of steady-state data the bifurcation diagram can be obtained by plotting

vertically the sampled output voltage whereas the voltage feedback gain is drawn horizontally as a control parameter.

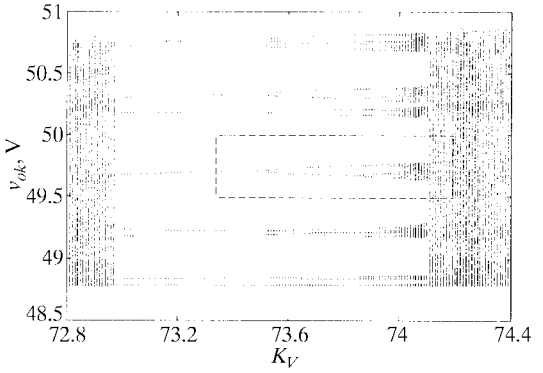

Fig. 25 Bifurcation diagram

The window encircled by dotted line in Figure 25 is shown in magnified form in Figure 26. Beautiful period doubling scenario can be seen again. Denoting the first bifurcation point by λ_0 where $\lambda_0 = K_V = 73.502$, the next one by λ_1 etc., the values of the first several bifurcation points are in Table 2.

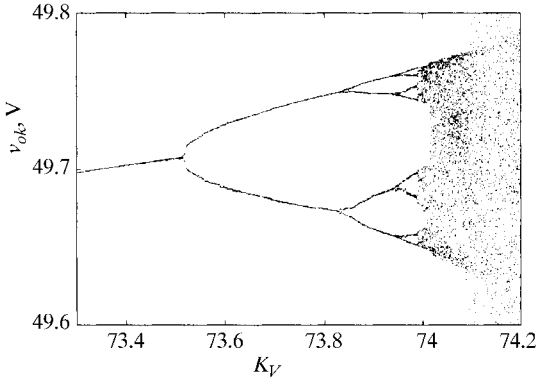

Fig. 26 Enlarged part of the bifurcation diagram

Table 2 contains δ_1 and δ_2. Even the first two δ values are not far from the Feigenbaum constant 4.66920161…

Table 2 **Bifurcation points in Figure 26**

k	λ_k	δ_k
0	73.501	
1	73.841	4.0476
2	73.925	4.2000
3	73.945	

The time function of condenser voltage v_c is plotted in Figure 27 at $K_V = 73.2$. The period-9 subharmonic state is clearly visible. The period of v_c, together with the period of the other state variables, is $9 * 2T = 9 * T_s$ in state period-9.

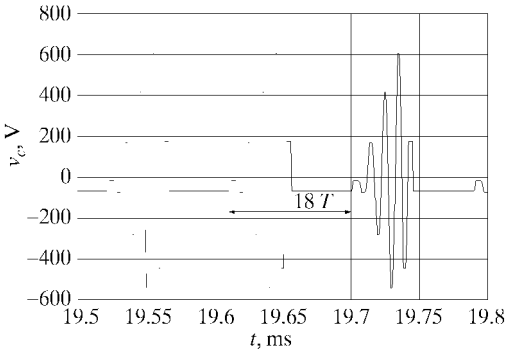

Fig. 27 Condenser voltage in period-9 operation

Figure 28 shows the Poincaré map for chaotic behavior at $K_V = 74.2$ in plane of output voltage $v_{ok} = v_o(kT_s)$ vs. inductor current $i_{opk} = i_{op}(kT_s)$. This map reveals a highly organized structure. Note also that it lies in a bounded region of state-space.

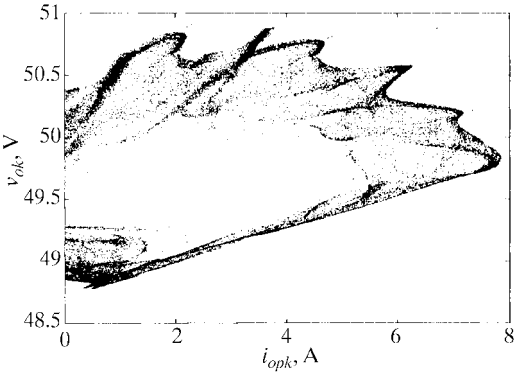

Fig. 28 Poincaré map for chaotic operation ($K_V = 74.2$)

SUMMARY

The paper has given a bird eye view of the advanced theory of nonlinear dynamical systems by overviewing their fundamental states and their stability. The four states mentioned are: fixed or equilibrium points, limit cycles, quasiperiodic states and chaotic states. Special attention was devoted to the routes to chaos, some tools for the investigation of chaos and the connection between chaos and fractal geometry. Three examples from the area of power electronics illustrated the presence of nonlinearity and chaos and the application of the advanced theory.

ACKNOWLEDGEMENTS

The author wishes to thank the Hungarian Research Fund (OTKA TO29026) and the Control Research Group of the Hungarian Academy of Science for their financial support.

REFERENCES

[1] I. Nagy, Z. Sütő, L. Matakas Jr, E. Masada, **Features of Adaptive PWM Explored by the Theory of Chaos**. /*.EPE'95, Sevilla, Spain, 19/21 September 1995, Vol. 2., pp. 1013–1018.

[2] F. C. Moon, **Chaotic and Fractal Dynamics**. John Wiley & Sons, New-York, USA, 1992.

[3] H. Peitgen, M. Jürgens, D. Saupe, **Chaos and Fractals**. Springer-Verlag, New-York, USA, 1993.

[4] J. R. Wood, **Chaos: A Real Phenomenon in Power Electronics**. IEEE APEC'89 Record, 115–124, 1989.

[5] J. H. B. Deane, D. C. Hamill, IEEE Trans. on Power Electronics, 5, 260–268, 1990.

[6] T. Ninomiya, A. Takeuchi, T. Kohama, **Beat Phenomenon, Phase-Lock, and Chaotic Oscillation in Resonant Converters**. Proceedings of Chinese/Japanese Power Electronics Conference, 1–8, 1992.

[7] H. Tsuboi, I. Vajda editor, **Study of Chaotic and Periodic Behaviours of a Hyteresis Current Controlled Induction Motor Drive**. Applied Electromagnetics and Computational Technology II. Book, I. Nagy, Z. Sütő (E) have written one chapter. Publisher IOS Press Ohmushu Ltd, Tokyo, Japan, 2000.

[8] Z. Sütő, I. Nagy, K. Zabán, **Nonlinear Current Control of Three Phase Converter**. /*, ISIE'98, Pretoria, South Africa, 7–10 July, 1998, Vol. 2, pp. 353–358.

[9] R. C. Hilborn, **Chaos and Nonlinear Dynamics**. Oxford University Press, 1994.

[10] I. Nagy, O. Dranga, Eisuke Masada, **Study of Subharmonic Generation In A High Frequency Time-Sharing Inverter.** The Transactions of The Institute of Electrical Engineers of Japan, A Publication of Industry Applications Society, Tokyo, Japan, 6 2000 pp. 574–580.

[11] I. Nagy, O. Dranga, E. Masada, **Bifurcations in a High Frequency Time-Sharing Inverter**. EPE-PEMC'2000 International Conference, 5–7 September 2000, Košice, Slovak Republic.

[12] I. Nagy, **Resonant DC-DC Configurations**. EPE'89. Third European Conference on Power Electronics. Vol. III. pp. 1495–1500. Aachen. W. Germany, 1989.

[13] I. Nagy, J. Hamar, I. Dénes, Z. Puklus, **Sliding Mode Control of a DC-DC Dual Channel Resonant Converter**. Proceedings of PCIM'2000 Conference Nürnberg, Germany, June 6–8, 2000.

[14] I. Nagy, P. Korondi, J. Hamar, **Design Considerations of a Two Channel DC-DC Resonant Converter**. /*, PEMC'98, Prague, Czech Republic, 8–10 September, 1998, Vol. 2, pp. 2–85–2–90.

[15] I. Nagy, P. Korondi, Z. Vranyecz, E. Masada, **Ratio Control of Two DC Power Flows in a New Resonant Converter Family**. /*,IPEMC'97, November 3–6, 1997, Hangzhou, China, Vol. 2, pp. 609–614.

[16] I. Nagy, O. Dranga, **Bifurcation in a Dual Channel Resonant DC-DC Converter**. ISIE'2000, 4–8 December 2000, Puebla, México.

[17] T. S. Parker, L. O. Chua, **Practical Numerical Algorithms for Chaotic Systems**. Springer-Verlag New York Inc., 1989.

[18] A. Lasota, M. C. Mackey, **Chaos, Fractals and Noise**. Applied Mathematical Sciences 97, Springer-Verlag New York Inc., 1994.

[19] E. Ott, **Chaos in Dynamical Systems**. Cambridge University Press, 1993.

[20] R. van Buskirk, C. Jeffries, **Observation of Chaotic Dynamics of Coupled Nonlinear Oscillators**. Phys. Rev. Journal, A 31(5), pp. 3332–3357, 1985.

[21] O. Woywode, **Dynamical Bifurcations and Invariant Densities in Power Electronic Systems**. Zur Erlangung des akademischen Grades eines Doktoringenieurs (Dr.-Ing.) vorgelegte Dissertation, Der Fakultat Elektrotechnik der Technische Universitat Dresden. 2000.

[22] S. Banerjee, G. C. Verghese, **Nonlinear Phenomena in Power Electronics**. Chapter 1, pp. 1–24, New York, 2001.

[23] M. C. Pera, B. Robert, C. Goeldel, **Nonlinear Dynamics in Electromechanical Systems – Application to a Hybrid Stepping Motor**. Electromotion, Vol. 7. No. 1, pp. 31–42, 2000.

[24] D. Carton, B. Robert, C. Goeldel, **Self-Similarity and Chaos in a Current Mode PWM-Bridge**. 6th International Conference ELECTRIMACS'99, pp. 109-114, Lisboa, Portugal, Sept. 14–16, 1999.

[25] S. E. Rivkin, D. B. Izosimov, S. V. Belkin, **Three-Phase Voltage Source Inverter With Feedforward Switching Losses Optimisation Technique**. PEMC'98, Vol. 2, pp. 2–68–2–73, Prague, Czech Republic, 8–10 September, 1998.

[26] J. Berkovich, A. Ioinovich, **Simulation of Chaotic Processes in Boost-Converters and Their Interpretation in Terms of Information Theory**. PEMC'98, Vol. 5, pp. 5–195–5–200, Prague, Czech Republic, 8–10 September, 1998.

[27] J. M. Hubé, D. Flieller, J-P. Louis, X. Quan, **Phase Locking Control of a Resonant DC-AC Converter**. EPE'97, Vol. 2, pp. 303–308, Trondheim, Norvegia, 8–10 September, 1997.

[28] M. M. Bech, J. K. Pedersen, F. Blaabjerg, **Random Modulation Techniques in Power Conversion – an Update**. PEMC'96, Vol. 3, pp. 357–365, Budapest, Hungary, 2–4 September, 1996.

[29] J. H. Chen, K. T. Chau, **Analysis of Chaos in Current-Mode-Controlled DC Drive Systems**, IEEE Trans on Industrial Electronics, Vol. 47, No. 1, pp. 67–76, February, 2000.

[30] M. di Bernardo, F. Vasco, **Discrete-Time Maps for the Analysis of Bifurcations and Chaos in DC/DC Converters**. IEEE Transactions on Circuits and Systems-Part I: Fundamental Theory and Applications, vol. 47, No. 2, February, 2000.

[31] M. P. Kazmierkowski, L. Malesani, **Current Control Techniques for Three-Phase Voltage-Source PWM Converters: A Survey**. IEEE Trans. on Industrial Electron. Vol. 45, No. 5. pp. 691–701, USA, 1998.

[32] M. Hartmann, J. Iwaszkiewicz, J. Perz, **A Floating Point DSP TMS320C31 Based Control of the Complex Inverter Structures**. PEMC'96, Vol. 1, pp. 336–340, Budapest, Hungary, 2–4 September, 1996.

[33] J. W. Kolar, H. Sree, U. Drofenid, Ned Mohan, F. C. Zach, **A Novel Three-Phase Three-Switch Three-Level High Power Factor SEPIC-Type AC-to-DC Converter**. 12th IEEE Applied Power Electronics Conference, pp. 1–9, Atlanta, USA, Feb. 23–27, 1996.

[34] I. Vajk, **Sensitivity of Nonlinear Dynamic Modeling**. Elsevier Science Ltd. Proceedings of 14th IFAC World Congress, vol H, pp. 19–24, Beijing, P. R. China, 1999.

[35] I. Vajk, **Biorthogonal Matrix Factorization Algorithms for Parameter Estimation**. 7th International Power Electronics and Motion Control (PEMC'96), Vol 2, pp 2/171–175, Budapest, Hungary, 2–4. Sept. 1996.

Nelinearne pojave u energetskoj elektronici. Nedavno je otkrivena nova vrsta pojava na području dinamike nelinearnih sustava. Novi pojmovi i nazivi zamijenili su vremenske funkcije i frekvencijske spektre u opisivanju njihovog ponašanja. U rječnik su uvedeni nazivi kao što su: kaos, bifurkacija, fraktal, Lyapunov koeficijent, period udvostručavanja, Poincaréov dijagram, nepoznati atractor, itd. Osnovni cilj članka je dati pregled sadašnjeg stanja napredne teorije nelinearnih dinamičkih sustava. S tri primjera ilustrirana je njezina primjenu u energetskoj elektronici.

Ključne riječi: dinamika nelinearnih sustava, teorija kaosa, putevi u kaos, geometrija fraktala, učinska elektronika

AUTHORS ADDRESS:

István Nagy, Research Professor,
Member of the Hungarian Academy of Sciences, IEEE Fellow

Budapest University of Technology and Economics,
Department of Automation and Applied Informatics
H-1111 Budapest, Budafoki út 8. HUNGARY,
E-mail: nagy@elektro.get.bme.hu
Computer and Automation Institute,
Hungarian Academy of Sciences

Received: 2001–07–12